PROCEEDINGS OF SCIENCE

# Exclusive Analysis of $p + p \rightarrow \Lambda + K_S^0 + p + \pi^+$ with HADES

**Snehankit Pattnaik,**[a,b,*] **Johan Messchendorp**[a] **and James Ritman**[a,b,c] **for the HADES collaboration**

[a] *GSI Helmholtzzentrum für Schwerionenforschung GmbH, Planckstraße 1, Darmstadt, Germany*

[b] *Fakultät für Physik und Astronomie, Ruhr-Universität Bochum, Universitätsstraße 150, Bochum, Germany*

[c] *Institut für Kernphysik (IKP), Forschungszentrum Jülich, Wilhelm-Johnen-Straße, Jülich, Germany*

*E-mail:* s.pattnaik@gsi.de, j.messchendorp@gsi.de, j.ritman@gsi.de

Strangeness production in proton-proton($pp$) collisions at $T = 4.5$ GeV with HADES is studied via the exclusive reaction $p + p \rightarrow \Lambda + K_S^0 + p + \pi^+$. A clear signature of $K^*(892)$ is extracted using a $\Delta$TOF-based PID and a sideband subtraction technique. Additionally, a missing-mass on proton selection enhances sensitivity to intermediate resonances, enabling a study of $N^* \rightarrow \Lambda K^*$. A pure three-body $\Lambda K^* p$ phase-space model fails to describe the data.

*The 21st International Conference on Hadron Spectroscopy and Structure (HADRON2025)*
*27 - 31 March, 2025*
*Osaka University, Japan*

*Speaker

 ISSN 1824-8039 . Published by SISSA Medialab.



PoS(HADRON2025)002

## 1. Introduction

The study of strangeness production at few-GeV energies improves our elementary knowledge of non-perturbative QCD in the SU(3) flavor sector. Moreover, it provides valuable constraints for event generators and transport models used as a basis for studies in heavy-ion collisions. This is particularly relevant for channels with a hyperon and a vector meson, which are sensitive to the poorly known $N^* \rightarrow YK^*$ branching ratios and to understand the interference between $s$-channel resonances and non-resonant mechanisms. These measurements complement previous photoproduction results and are relevant for baryon spectroscopy [1, 2].

The present work investigates the exclusive reaction

$$p + p \rightarrow \Lambda + K^0_S + p + \pi^+,$$

at a proton kinetic beam energy of $T = 4.5$ GeV ($\sqrt{s} = 3.46$ GeV). This final state contains the vector meson $K^*(892) \rightarrow K^0_S\pi^+$ and is therefore directly sensitive to the $\Lambda K^*$ subsystem, where intermediate $N^*$ resonances may contribute. At these energies, channels such as $\Sigma^* \rightarrow \Lambda\pi^+$ and $\Delta^{++} \rightarrow p\pi^+$ overlap kinematically and can populate the region of interest. A proper assessment of competing channels and, ultimately, an amplitude analysis are therefore necessary to understand the production mechanism and to extract resonance contributions in the 2.0-2.5 GeV mass region.

Previous studies with HADES at $T = 3.5$ GeV and other fixed-target experiments at higher energies have established reference measurements for strangeness production in $pp$ collisions, such as $pK^+\Lambda$, and have highlighted the role of intermediate $N^*$ states and non-resonant contributions in related channels [3]. However, $\Lambda K^*$ channel in hadronic reactions at SIS18 energies remains largely unexplored, motivating a dedicated measurement with a large acceptance such as provided at the High Acceptance Di-Electron Spectrometer (HADES).

## 2. Experiment

The measurements presented here were carried out with HADES at the GSI Helmholtzzentrum für Schwerionenforschung in Darmstadt, Germany. Proton beams from the SIS18 synchrotron were delivered at a kinetic energy of 4.5 GeV [4].

The experimental detector setup shown in Fig. 1, combines several complementary sub-systems enabling a precise track and event reconstruction. Charged particle tracking is performed by four planes of multi-wire drift chambers (MDC), located before and after the magnetic field region, which allow precise momentum reconstruction. The time-of-flight (TOF) measurements are provided by scintillator walls and resistive plate chambers (RPC), using the TOF and RPC detectors respectively, which cover a total angular region from $\theta = 18°$ to $\theta = 85°$. Together with the precise TOF measurement and the momentum reconstruction, a preliminary particle identification is obtained. The forward straw tracking stations extend the acceptance into the small angular region, from $\theta = 0.5°$ to $\theta = 7°$, which is particularly relevant for hadronic channels and hyperon production at these beam energies. The forward detector operates in a magnetic field-free region and does not provide a direct momentum reconstruction; therefore, all forward tracks are assumed to be protons, with their momentum calculated from the measured flight path and TOF. Electron identification is ensured by a Ring Imaging Cherenkov (RICH) detector placed upstream to the superconduction

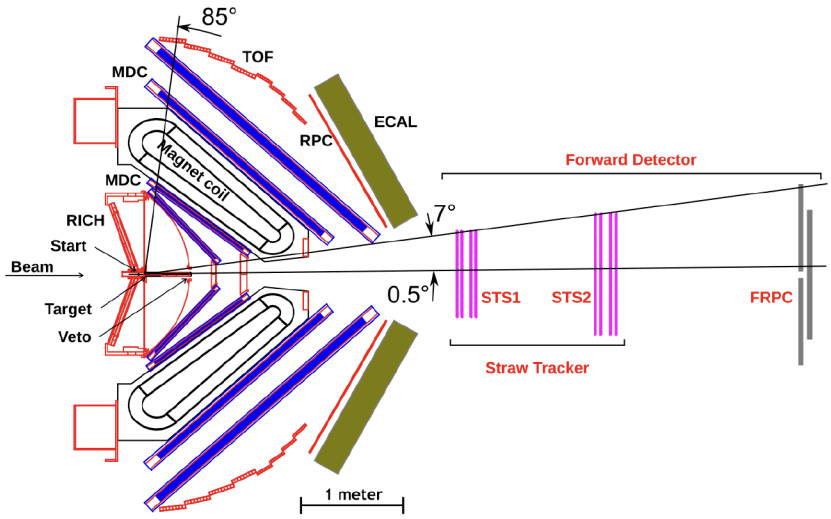


**Figure 1:** Schematic layout of the HADES spectrometer used during the $pp$ collision experiment at T = 4.5 GeV as presented in this work [5].

toroidal magnet, in a field-free zone, while the electromagnetic calorimeter is placed downstream, responsible for photon detection.

For the experiment discussed here, a proton beam with an average intensity of about $7.5 \times 10^7$ particles per second was directed on a liquid-hydrogen target of roughly 5 cm in length. This configuration yielded a data set of approximately $1.5 \times 10^9$ events recorded with a time-integrated luminosity of $\mathcal{L} = (5.86 \pm 0.06)$ pb$^{-1}$ at HADES [5].

## 3. Analysis Techniques

The analysis presented here discusses the reconstruction of the exclusive channel, which was primarily based on a reconstruction of $\Lambda K^0_S \pi^+$ system through a missing-mass of a proton. A complete exclusive analysis by reconstructing all six charged tracks is presented in FAIRness2024 [6]. The missing-mass method relies on the momentum information from the deviation in the magnetic field of the tracks reconstructed using the drift chambers. Events with a well reconstructed global vertex and start-time ($t_0$) measurement were selected.

To improve the reconstruction of this exclusive analysis, particle identification (PID) of the charged tracks was performed using the TOF and RPC detectors. Negatively charged tracks were dominated by $\pi^-$ mesons and at least two tracks were accepted with a minimum velocity cut of $\beta > 0.4$. Each event required a minimum of four positively charged particles, where both $\pi^+$ and protons are found in an overlapping momentum region ($\beta$ vs $p$ analysis), a relative ToF method was applied. The expected flight time for a given mass hypothesis was calculated from the reconstructed momentum and path length, the measured TOF was obtained from the TOF detector systems. The $\Delta$TOF was defined as the difference between the measured and the expected TOF for a given mass hypothesis. The reconstructed information of the tracks from $\pi^-$ candidates were used as a reference clock to eliminate the start time dependence for the positive tracks, by taking the average of the two $\pi^-$ candidates, resulting in a relative TOF measurement for each candidate.

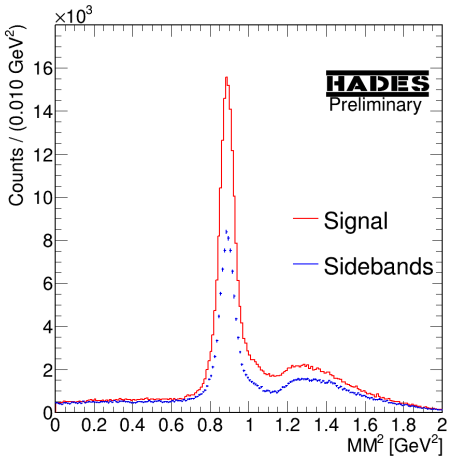


**Figure 2:** Missing-mass squared distribution of the $\Lambda K^0_S \pi^+$ system, resulting in a missing proton. The red histogram shows the inclusive yield in signal region around the $\Lambda K^0_S$ nominal mass, while the blue histogram represents the averaged sideband contribution.

Subsequently, the missing mass of the $\Lambda K^0_S \pi^+$ subsystem was then calculated by assuming different mass hypotheses for the charged tracks, e.g. $M(p)$ and $M(\pi)$. Cycling through different permutations, events that produced a missing mass close to the proton mass were retained, ensuring that only candidates consistent with the exclusive $p+p \rightarrow \Lambda+K^0_S+p+\pi^+$ reaction were considered. This requirement effectively suppressed non-exclusive background contributions and provided a clean starting point for further analysis.

All possible assignments of a protons and two $\pi^+$ were tested, and the configuration with the smallest overall sum of relative TOF was chosen as the most probable PID hypothesis. Through this combination of a missing-mass constraint and a relative TOF-based PID method, a high-purity sample of the exclusive final state was obtained for the neutral candidate reconstruction.

To reconstruct the neutral $K^0_S$ and $\Lambda$ candidates, four different combinations are assessed to identify, $\Lambda \rightarrow p\pi^-$ and $K^0_S \rightarrow \pi^+\pi^-$. Here, the missing proton is assumed to be the primary proton, originating from the interaction vertex, since the proton from the $\Lambda$ decay has a poorer resolution due to the limited resolution in the beam direction in HADES. After the coincident reconstruction of the invariant mass distributions of this pair neutral candidates, a sideband subtraction method is followed to remove non-resonant background and contributions from other channel. The sideband subtraction is performed by defining the signal region as a $\pm 3\sigma$ window around the nominal mass of the neutral candidates while the sidebands with the same width are used to estimate the average combinatorial background. Fig. 2 shows the reconstructed missing mass of the $\Lambda K^0_S \pi^+$ system (proton missing) in red, while the sideband histogram in blue shows the non-resonant background, contributions from other background channels such as $\pi\, p(n)$ bump is seen in the 1.2 GeV$^2$ region.

This subtraction procedure was also applied to the invariant-mass distributions of intermediate resonances. $K^*(892)$ was reconstructed by combining the primary $\pi^+$ with the neutral candidate $K^0_S$, resulting in a clean yield after the background removal as shown in Fig. 3a. Subsequently, the $M(\Lambda K^0_S)$ and $M(\Lambda K^*)$ invariant masses are extracted to study the role of intermediate resonances.

To validate the analysis and provide acceptance corrections, phase-space Monte Carlo samples were generated for several reaction channels using the Pluto event generator [7]. These included the pure phase-space process $p + p \rightarrow \Lambda + K^0_S + p + \pi^+$, as well as channels with intermediate resonances such as $p + p \rightarrow \Lambda + K^*(\rightarrow K^0_S\pi^+) + p$, $p + p \rightarrow \Lambda + K^0_S + \Delta^{++}(\rightarrow p\pi^+)$ and $p + p \rightarrow \Sigma^*(\rightarrow \Lambda\pi^+) + K^0_S + p$. The detector response was modeled using Geant3 [8], and the simulated events were analyzed with the same reconstruction and selection criteria as applied to the experimental data [6].

The contribution of $K^*(892)$ decays was obtained using a sideband analysis of events around the $K^0_S\pi^+$ invariant mass. The signal region was defined as a $\pm 2\sigma$ window around the nominal $K^*(892)$ mass, while two sidebands of half the signal width were placed symmetrically on either side. The background estimate from the sidebands therefore were the sum of the two sideband regions. Therefore, after the sideband subtraction, this procedure largely removes combinatorial and cross-channel contributions, including events from the $\Delta^{++}$ and $\Sigma^*$ channels, leaving only the $K^*$ channel.

## 4. Results

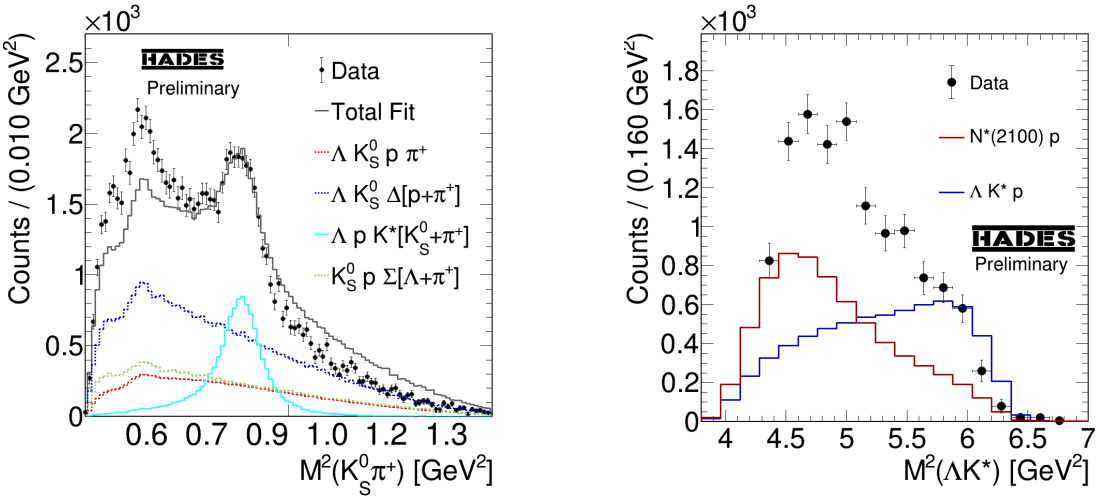


**(a)** **(b)**

**Figure 3:** Reconstructed distributions of $M^2(\pi^+K^0_S)$ (a) along with their relative contributions from the underlying intermediate 3-body and 4-body phase space contributions. The sideband-corrected data (b) are shown as black markers.

The observed $K^0_S\pi^+$ mass distribution, as depicted in Fig. 3a, shows a clear signal of $K^*(\rightarrow \pi^+ + K^0_S)$ decays. The peak position coincides with the expected mass as report by the Particle Data Group [9]. This justifies the assumption of taking a sum of the two sidebands in the $K^*$ background, as it largely follows a linear pattern as seen in Fig. 3a. Figure 3b shows the invariant-mass squared distribution of the $\Lambda K^*$ system. The data (filled circles) are compared to results of Monte Carlo simulations for $pp \rightarrow pK^*\Lambda$. The error bars account only for the statistical uncertainties. The blue histogram represents the results of a three-body phase-space model accounting for the detector

acceptance and reconstruction efficiency of the $\Lambda K^* p$ final state. The data are incompatible with a pure phase-space description, even after normalizing the simulation to match the total number of data events by integrating over the displayed range. To account for a $t$-channel contribution, events from the three-body sample were weighted with a Breit-Wigner line shape for an $N^*(2100) \to \Lambda K^*$ decay, without including possible interference terms. The resulting histogram in red follows the general trend of the data but there could be additional $N^*$ contributions or interference among overlapping broad resonances. As several broad resonance states lie around the same mass, an incoherent treatment is insufficient. Therefore the next step is to perform a more complete amplitude fit for drawing definitive conclusions.

## 5. Conclusion

We reported preliminary results of an analysis of the reconstruction of the exclusive $p + p \to \Lambda + K^0_S + p + \pi^+$ channel at $T = 4.5$ GeV using a missing-mass selection on the proton. Additionally, a $\Delta$TOF-based PID and a sideband subtraction on $M(K^0_S\pi^+)$ have been applied to extract the $K^*(892)$ yield. Clearly, the reconstructed three-body phase-space model on the $M^2(\Lambda K^*)$ spectrum fails to describe the data. A simple a Breit–Wigner model for $N^*(2100) \to \Lambda K^*$ improves the overall shape but there could be additional dynamics among overlapping contributions.

These observations indicate a requirement for a complete amplitude analysis. An ongoing study is therefore implementing an amplitude fit within the Jülich–Bonn (JuBo) framework to quantify the relative contributions of $t$-channel $N^*$ states and non-resonant mechanisms that decay to $\Lambda + K^0_S + p + \pi^+$ in their final states [10].

## References

[1] S.-H. Kim, *Phys. Rev. D* **90**, 014021 (2014).

[2] A. C. Wang, *Phys. Rev. C* **96**, 035206 (2017).

[3] R. Abou Yassine *et al.*, Eur. Phys. J. A **60**, 18 (2024).

[4] G. Agakichiev *et al.*, Eur. Phys. J. A **41**, 243–277 (2009).

[5] J. Adamczewski-Musch *et al.*, Eur. Phys. J. A **57**, 138 (2021).

[6] S. Pattnaik *et al.*, arXiv:2509.04937.

[7] I. Fröhlich *et al.*, J. Phys Conf. Ser. **219** 032039 (2010).

[8] Y. Zheng-Yun *et al.*, Chinese Phys. C **32** 572 (2008).

[9] P.A. Zyla *et al.*, (Particle Data Group), Prog. Theor. Exp. Phys. **2020**, 083C01 (2020).

[10] D. Rönchen *et al.*, Eur. Phys. J. A **54**, 110 (2018).